Discriminating Between sMRI and fMRI Brain Networks using Centrality Measures and Deep Graph Neural Networks

Batuhan K. Karaman*†‡§, Alan Q. Wang *†§,
*School of Electrical and Computer Engineering, Cornell University and Cornell Tech, New York, NY 10044
†Department of Radiology, Weill Cornell Medicine, New York, NY 10021
‡ kbk46@cornell.edu
§ indicates equal contribution

***Abstract*—We seek to analyze brain networks derived from MRI measurements and quantify the discriminative power of centrality measures of these networks for the task of classifying between structural (sMRI) and functional MRI (fMRI). We pass a graph with node features derived from various centrality measures as input into a deep graph neural network, which is trained to classify networks as being derived from sMRI or fMRI measurements. These graphs are extracted from a brain network, where each node represents a region of the brain and each edge weight is proportional to the correlation of brain activity between two regions. We use a real-world dataset consisting of pairs of sMRI and fMRI signals from a set of subjects.**

I. Introduction

The phenomenon of nuclear magnetic resonance imaging (NMRI) was first observed in 1945 [1], [2]. It was the injection of radiofrequency engineering expertise and the availability of stable new frequency sources, both byproducts of the wartime development of radar, which probably made the demonstration of NMRI possible. NMRI imaging was first reported in 1973 [3], [4] and the first human in vivo MRI images were produced by the end of that decade. Compared with images from other modalities, MRI images of the head provided excellent anatomical detail and strong grey/white matter contrast. Today, coronal T1-weighted, three-dimensional, high-resolution images are used to measure the volume of the hippocampus, usually by means of manually tracing its outline. They are also the basis for many cross-sectional and longitudinal studies determining the volume of, and assessing changes in, the hippocampus over time in hippocampal sclerosis and Alzheimer's disease.

The division between structural and functional imaging is difficult to make because structure and function are often inextricably intertwined in the brain. Definitions of functional imaging are varied and often broad and will always be arbitrary to a certain extent. On the basis of biological considerations, functional imaging can be regarded as the method providing dynamic physiological information, whereas structural imaging provides static anatomical information. Functional magnetic resonance imaging (fMRI) [5], [6] measures brain activity by detecting changes related to blood flow. This technique is based on the fact that cerebral blood flow and neuronal activation are combined. When an area of the brain is used, blood flow to that area also increases [7]. The primary form of fMRI using blood oxygen-dependent contrast (BOLD), was discovered in 1990 by Seiji Ogawa. This is a type of specialized brain and body scan used to map neural activity in the brain or spinal cord of humans or other animals by imaging the change in blood flow (hemodynamic response) related to energy use by brain cells. Since the early 1990s, fMRI has dominated brain mapping research because it does not involve the use of injections, surgery, oral substances, or exposure to ionizing radiation. This measurement is frequently subject to interference from various sources; therefore, statistical procedures are used to extract the underlying signal. Brain activation results can be graphically represented by color coding the intensity of activation on the specific brain or region being studied. This technique can locate the operation within millimeters, but when using standard techniques, no better within a few seconds window. Other methods to obtain contrast are arterial labeling [8] and MRI diffusion. Diffusion MRI is similar to BOLD fMRI but provides contrast based on how diffusely water molecules are present in the brain. Task-based fMRI (T-fMRI) measures BOLD signal changes between task-stimulated states and control states.

In addition to detecting BOLD responses from task or stimulus-induced activity, fMRI can measure either resting or negative task states, showing the subject's baseline variance BOLD. Resting-state FMRI (R-fMRI) [9] is a functional magnetic resonance imaging (fMRI) method used in brain mapping to evaluate regional interactions that occur during resting or an inactive task [10], [11]. Several resting brain networks have been identified, one of which is the default mode network. These brain networks are observed through changes in blood flow in the brain, producing a signal known as a blood oxygen level-dependent (BOLD) signal that can be measured by fMRI. Since brain activity is intrinsic, present even in the absence of an externally requested task, any region of the brain will experience spontaneous fluctuations in the BOLD signal. The resting-state approach is useful for exploring the functional organization of the brain and examining whether it is altered in neurological or psychiatric disorders. Due to the resting-state aspect of this imaging, data can be collected from a variety of patient groups, including

those with intellectual disabilities, groups of children, and even unconscious individuals [12], [13]. Resting-state functional connectivity research has revealed a number of networks that are consistently found in healthy subjects, at different stages of consciousness, and across species, and represent specific patterns of synchronous activity.

II. Brief explanation of the problem

In this project, we seek to classify between structural connectivity (SC) and functional connectivity (FC) signals in MRI. Our networks in this work are connectivity matrices, where each node represents a region of the brain and the edge weights are proportional to the correlation of brain activity between two regions. For node features, we experiment with several different centrality measures, including degree, eigenvector, closeness, and information. We build a graph convolutional network (GCN) that takes these connectivity matrices as input and outputs the prediction of whether the matrix is derived from a structural or functional connectivity matrix. We use classification accuracy and the area under the receiver operating characteristics curve (AUC) to compare the predictive performance of these classifiers.

The centrality measures we choose can be categorized by whether or not they leverage the edge weight information. Degree, closeness, and unweighted eigenvector centrality measures do not use edge weight information (i.e. they treat the edges as binary), while weighted eigenvector and information centrality measures do. We refer to the first group as nonweighted centrality measures and the second group as weighted centrality measures. We hypothesize that weighted centrality measures should be more useful as node features for this task. This is because much of the variability between structural and functional MRI signals is in the differences in relative brain function between different regions of the brain. Thus, features that leverage this difference (which is encoded in the edge weights) should be more discriminate than features that do not.

III. Proposed Method

A. Node Embeddings

We consider the following node embeddings ϕ for node v:

1) Degree Centrality: The embedding of the node is equivalent to its degree:

$$\phi(v) = \deg(v). \tag{1}$$

2) Unweighted Eigenvector Centrality: Eigenvector centrality computes the centrality of a node based on the centrality of its neighbors. The eigenvector centrality for node i is the i-th element of the vector x defined by the equation

$$Ax = \lambda x, \tag{2}$$

where A is the adjacency matrix of the graph with eigenvalue λ.

In the unweighted variant, we treat A as a (symmetric) binary matrix with entries in $\{0, 1\}$. In the weighted variant, A is a (symmetric) matrix with entries equal to the edge weights.

3) Closeness Centrality: The embedding is the (normalized) inverse distance to all other nodes in the graph:

$$\phi(v) = \frac{N-1}{\sum_u d(u,v)}, \tag{3}$$

where $d(u, v)$ is the distance between vertices u and v.

4) Information Centrality: Also known as current-flow closeness centrality, information centrality is a variant of closeness centrality based on effective resistance between nodes in a network [14]:

$$\phi(v) = (NC_{vv} + +\text{trace}(C) - 2/N)^{-1}, \tag{4}$$

where $C = (L + J)^{-1}$, L is the Laplacian, and $J = \mathbf{1}\mathbf{1}^T$.

B. Model

We wish to design a model that maps a given graph $\mathcal{G}$ to a scalar in $[0, 1]$. We use a graph convolutional network with ℓ graph convolution layer, a readout layer, and a final dense classifier with sigmoid activation.

The graph convolution layer we use is first presented in [15]. It performs the operation

$$H^{\ell+1} = \sigma(\tilde{D}^{-1/2}\tilde{A}\tilde{D}^{-1/2}H^{\ell}W^{\ell}), \tag{5}$$

where $\tilde{A} = A + I_N$ is the adjacency matrix of the undirected graph with added self-connections, I_N is the identity matrix, $\tilde{D}_{ii} = \sum_j \tilde{A}_{ij}$, X is the node embeddings, and W^{ℓ} is the layer-specific trainable weight matrix. σ is a nonlinear activation function, which we choose as the ReLU function: $ReLU(x) = \max(0, x)$. This operation can be viewed as a propagation rule for the localized first-order approximation of a spectral graph convolution. Effectively, these layers embed each node by performing multiple rounds of message passing.

The readout layer aggregates node embeddings into a unified graph embedding. We choose a simple average of node embeddings as the readout layer:

$$e_{\mathcal{G}} = \frac{1}{|\mathcal{V}|}\sum_{v\in\mathcal{V}} e_v, \tag{6}$$

where e_v is the learned embedding for each node.

Finally, a dense layer maps the aggregated embedding to a scalar with an additional bias, which is followed by a sigmoid activation:

$$p = \text{sigmoid}(w^T e_{\mathcal{G}} + b). \tag{7}$$

In this case, w is a column vector of trainable weights and b is a trainable bias scalar.

C. Loss

We train the model by minimizing the binary cross-entropy loss:

$$\mathcal{L} = -\sum_{i=1}^{N} \left[y_i \log(p_i) + (1 - y_i) \log(1 - p_i) \right], \tag{8}$$

where y is the label of the input graph and i indexes over a dataset of N graph-label pairs.

IV. Experiments

A. Dataset

The data for this project comes from the publicly available HCP database containing high-resolution, preprocessed anatomical, diffusion, and resting-state functional MRI data. Specifically, we use WU-Minn HCP minimally processed S1200 release which includes high-resolution 3T MR scans, demographics, and behavioral and cognitive scores for a population of 1113 young healthy adults (age 22 to 37 years).

1) Construction of the Structural Connectomes: HCP subjects were scanned on a customized Siemens 3T "Connectome Skyra" housed at Washington University in St. Louis. The HCP diffusion data (1.25mm isotropic voxels, TR/TE = 5520/89.5ms, 3x multiband acceleration, b=1000,2000,3000, 90 directions/shell, collected with both left-right and right-left phase encoding) were first minimally preprocessed by the HCP consortium to correct for motion, EPI and eddy-current distortion, and registered to each subject's T1 anatomical scan [16]. We used a probabilistic (iFOD2 [17]), anatomically constrained (ACT [18]) tractography algorithm with dynamic white-matter seeding to create individual, whole-brain tractograms containing 5 million streamlines for each subject. The SC between any two regions was the SIFT2-weighted sum of streamlines connecting those regions divided by the sum of the gray matter volume of those regions. The result was an ROI-volume normalized pairwise SC matrix for each subject.

2) Construction of the Functional Connectomes: There were four gradient-echo EPI resting-state fMRI runs (2.0mm isotropic voxels, TR/TE = 720/33.1ms, 8x multiband acceleration, FoV = 208×180 mm^2, FA = 52°, 72 slices) of approximately 15 minutes each, with two runs in one session and two in a second session, where each session included both right-left and left-right phase encoding. There were 1200 volumes for each run and a total of 4800 volumes (1200 volumes $\times$ 4 runs) for each subject. The data were minimally preprocessed [16] and ICA+FIX [19], [20] denoised by the HCP consortium [21]. FC matrices were calculated using the Pearson correlation between each region-pair's average time series in the CC400 atlas [22], resulting in four FC matrices for each subject.

B. Model and Training Details

For nonweighted centrality measures, we use one graph convolution layer. For weighted centrality measures, we use two graph convolution layers. The hidden channels of the convolution layer are 64.

For training, we use the Adam optimizer with a learning rate of 0.01, and a batch size of 4. We use a 50/50 train/test split.

C. Metrics

We evaluate our model using two metrics: accuracy (Acc) and the area under the receiver operating characteristics curve (AUC).

TABLE I
Summary of results. Accuracy and AUC for all node centrality embeddings.

Model	Acc (%)	AUC (%)
Degree	100.0	100.0
Eigenvector	100.0	100.0
Closeness	100.0	100.0
Weighted Eigenvector	100.0	100.0
Information	99.2	100.0

D. Results

Table I shows the main results. We find that all models can achieve perfect accuracy and AUC on this task, except for Information. We hypothesize that this is due to the information centrality measure being sensitive to noise, or a lack of model capacity due to the increased information represented in the node features.

Figures 1, 2, 3, 4, and 5 show loss, accuracy, and AUC curves across training. We generally observe the convergence of the network within 20-30 epochs for the nonweighted centrality measures, and the jump to zero loss occurs quite suddenly. On the other hand, weighted eigenvector and information centrality measures take longer to converge. The weighted eigenvector has a smoother loss curve, while the loss of the information centrality is jumpy, perhaps indicating the presence of noise in the inputs that the centrality measure emphasizes.

V. Discussion and Conclusion

We train a GCN model to classify structural and functional fMRI brain signals, using various graph centrality measures as node features. We find that nonweighted centrality measures outperform weighted centrality measures in terms of end classification performance, contrary to our initial hypothesis. We attribute this to the fact that although the nonweighted centrality measures do not leverage edge weight information, this information is still propagated through the GCN model via A in Eq. (5). In fact, the performance for weighted centrality measures may suffer because the features may be more sensitive to noise, or may cause the model to underfit due to the increased complexity. Indeed, during our experiments, we increased the number of graph convolution layers for the weighted centrality measures in order to achieve (near) equivalent results to the nonweighted measures. Nevertheless, we conclude that simple, nonweighted centrality measures are sufficient node features for this task.

We believe our method offers automated classification of fMRI connectivity types and provides insights into the most useful features for distinguishing structural and functional brain signals, particularly through the use of simple centrality measures and a robust graph neural network.

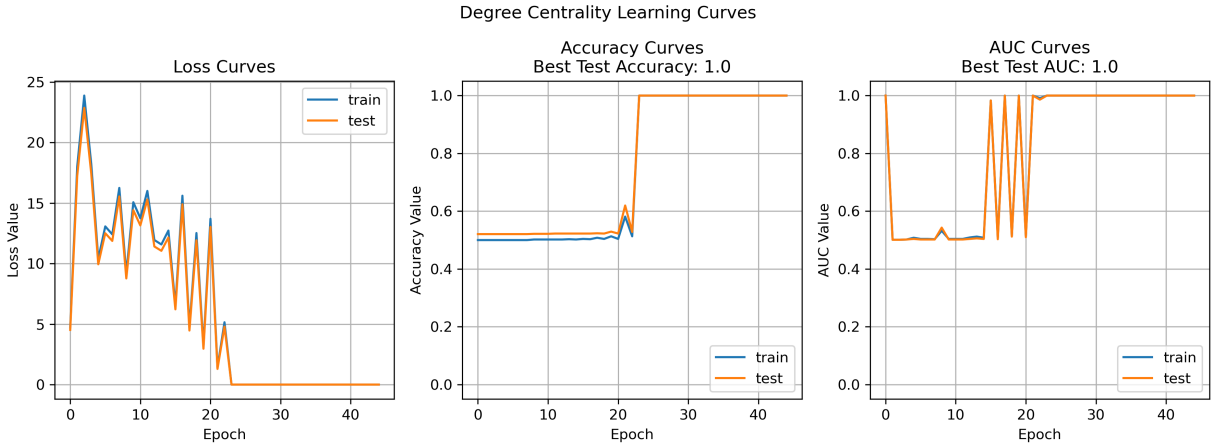

Fig. 1. Learning curves with degree centrality as node embeddings.

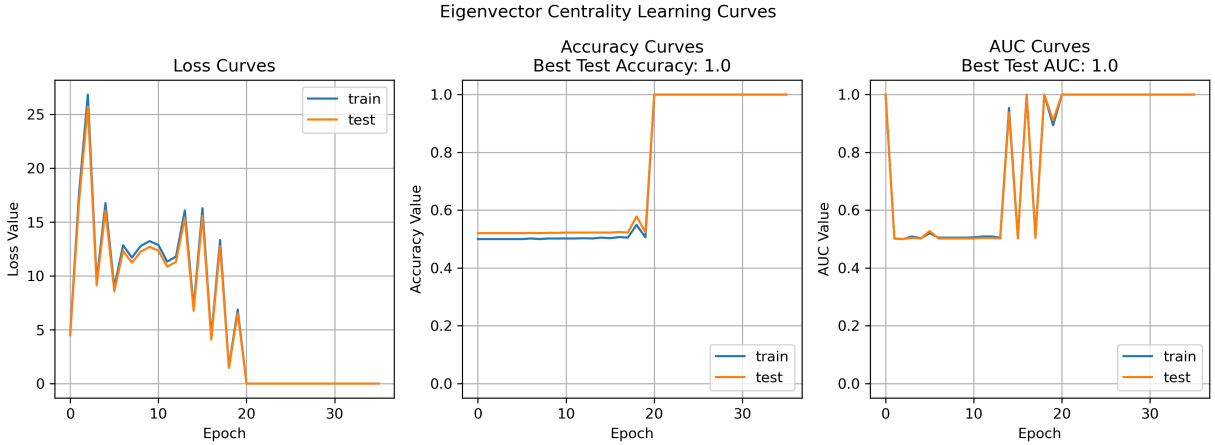

Fig. 2. Learning curves with unweighted eigenvector centrality as node embeddings.

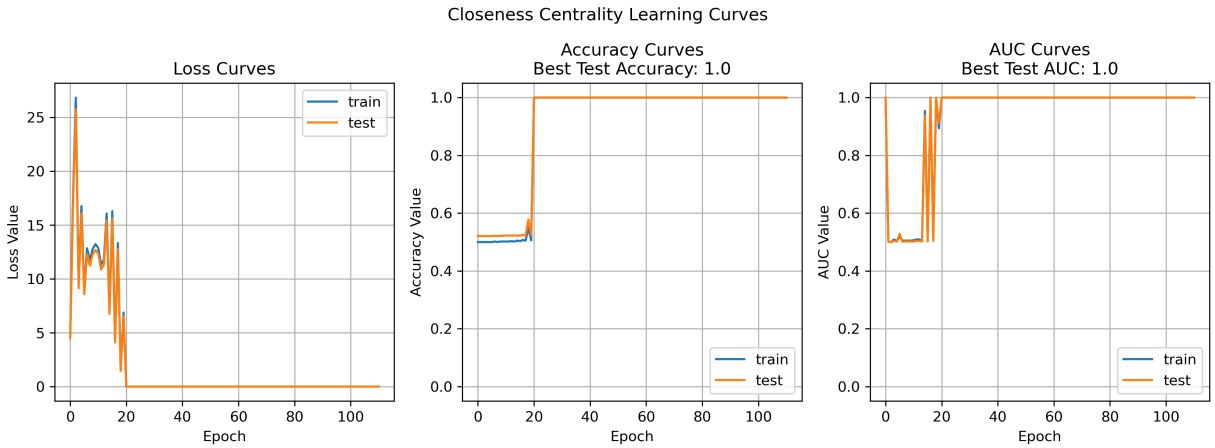

Fig. 3. Learning curves with closeness centrality as node embeddings.

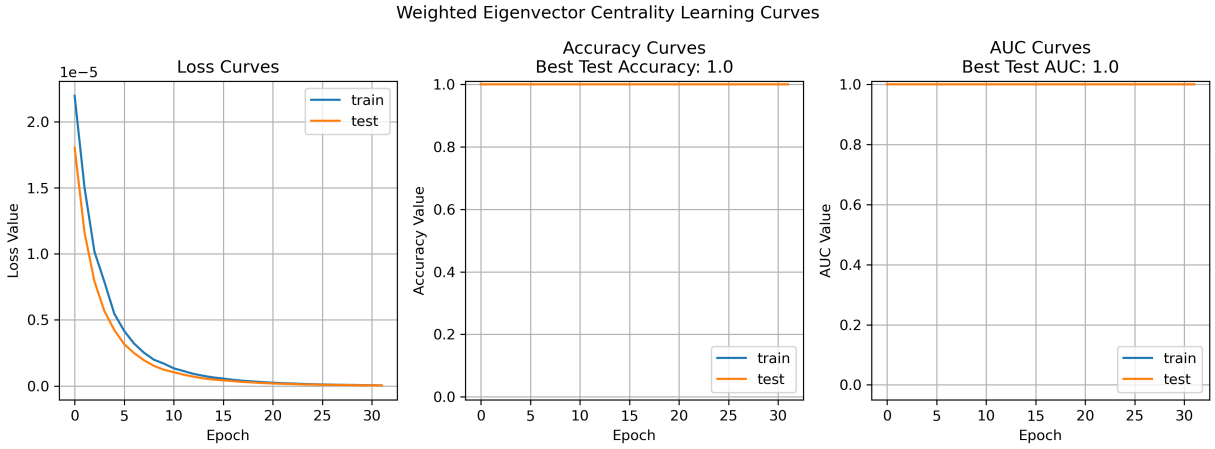

Fig. 4. Learning curves with weighted eigenvector centrality as node embeddings.

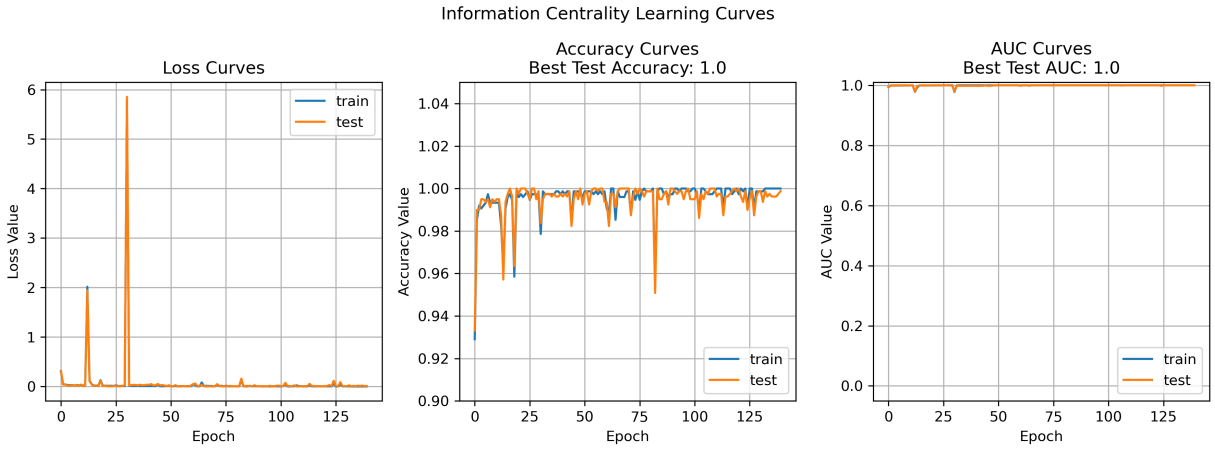

Fig. 5. Learning curves with information centrality as node embeddings.

REFERENCES

[1] F. Bloch, "Nuclear induction," *Physical Review*, vol. 70, pp. 460–474, 10 1946.

[2] E. M. Purcell, H. C. Torrey, and R. V. Pound, "Resonance absorption by nuclear magnetic moments in a solid," *Physical Review*, vol. 69, pp. 37–38, 01 1946.

[3] P. Mansfield and P. K. Grannell, "Nmr 'diffraction' in solids?," *Journal of Physics C: Solid State Physics*, vol. 6, pp. L422–L426, 11 1973.

[4] P. C. LAUTERBUR, "Image formation by induced local interactions: Examples employing nuclear magnetic resonance," *Nature*, vol. 242, pp. 190–191, 03 1973.

[5] P. M. Matthews and P. Jezzard, "Functional magnetic resonance imaging," *Journal of Neurology, Neurosurgery & Psychiatry*, vol. 75, p. 6–12, 01 2004.

[6] M. J. Singleton, "Functional magnetic resonance imaging," *The Yale Journal of Biology and Medicine*, vol. 82, p. 233, 12 2009.

[7] N. K. Logothetis, J. Pauls, M. Augath, T. Trinath, and A. Oeltermann, "Neurophysiological investigation of the basis of the fmri signal," *Nature*, vol. 412, pp. 150–157, 07 2001.

[8] J. A. Detre, H. Rao, D. J. Wang, Y. F. Chen, and Z. Wang, "Applications of arterial spin labeled mri in the brain," *Journal of Magnetic Resonance Imaging*, vol. 35, pp. 1026–1037, 01 2012.

[9] S. M. Smith, C. F. Beckmann, J. Andersson, E. J. Auerbach, J. Bijsterbosch, G. Douaud, E. Duff, D. A. Feinberg, L. Griffanti, M. P. Harms, M. Kelly, T. Laumann, K. L. Miller, S. Moeller, S. Petersen, J. Power, G. Salimi-Khorshidi, A. Z. Snyder, A. T. Vu, M. W. Woolrich, J. Xu, E. Yacoub, K. Uğurbil, D. C. Van Essen, and M. F. Glasser, "Resting-state fmri in the human connectome project," *NeuroImage*, vol. 80, pp. 144–168, 10 2013.

[10] B. B. Biswal, "Resting state fmri: A personal history," *NeuroImage*, vol. 62, pp. 938–944, 08 2012.

[11] R. L. Buckner, F. M. Krienen, and B. T. T. Yeo, "Opportunities and limitations of intrinsic functional connectivity mri," *Nature Neuroscience*, vol. 16, p. 832–837, 07 2013.

[12] O. Agcaoglu, T. W. Wilson, Y. Wang, J. Stephen, and V. D. Calhoun, "Resting state connectivity differences in eyes open versus eyes closed conditions," *Human Brain Mapping*, vol. 40, pp. 2488–2498, 02 2019.

[13] K. Smitha, K. Akhil Raja, K. Arun, P. Rajesh, B. Thomas, T. Kapilamoorthy, and C. Kesavadas, "Resting state fmri: A review on methods in resting state connectivity analysis and resting state networks," *The Neuroradiology Journal*, vol. 30, pp. 305–317, 03 2017.

[14] U. Brandes and D. Fleischer, "Centrality measures based on current flow," in *STACS 2005* (V. Diekert and B. Durand, eds.), (Berlin, Heidelberg), pp. 533–544, Springer Berlin Heidelberg, 2005.

[15] T. N. Kipf and M. Welling, "Semi-supervised classification with graph convolutional networks," *arXiv:1609.02907 [cs, stat]*, 02 2017.

[16] M. Glasser, S. Sotiropoulos, J. Wilson, T. Coalson, B. Fischl, J. Andersson, J. Xu, S. Jbabdi, M. Webster, J. Polimeni, D. Van Essen, and M. Jenkinson, "The minimal preprocessing pipelines for the human connectome project," *NeuroImage*, vol. 80, pp. 105–124, Oct. 2013.

[17] J.-D. Tournier, F. Calamante, and A. Connelly, "Improved probabilistic streamlines tractography by 2nd order integration over fibre orientation distributions," *Proc. Intl. Soc. Mag. Reson. Med. (ISMRM)*, vol. 18, 01 2010.

[18] R. E. Smith, J.-D. Tournier, F. Calamante, and A. Connelly, "Anatomically-constrained tractography: Improved diffusion mri streamlines tractography through effective use of anatomical information," *NeuroImage*, vol. 62, pp. 1924–1938, 09 2012.

[19] L. Griffanti, G. Salimi-Khorshidi, C. F. Beckmann, E. J. Auerbach, G. Douaud, C. E. Sexton, E. Zsoldos, K. P. Ebmeier, N. Filippini, C. E. Mackay, S. Moeller, J. Xu, E. Yacoub, G. Baselli, K. Ugurbil, K. L. Miller, and S. M. Smith, "Ica-based artefact removal and accelerated fmri acquisition for improved resting state network imaging," *NeuroImage*, vol. 95, pp. 232–247, 2014.

[20] G. Salimi-Khorshidi, G. Douaud, C. F. Beckmann, M. F. Glasser, L. Griffanti, and S. M. Smith, "Automatic denoising of functional mri data: Combining independent component analysis and hierarchical fusion of classifiers," *NeuroImage*, vol. 90, pp. 449–468, 2014.

[21] S. M. Smith, C. F. Beckmann, J. Andersson, E. J. Auerbach, J. Bijsterbosch, G. Douaud, E. Duff, D. A. Feinberg, L. Griffanti, M. P. Harms, M. Kelly, T. Laumann, K. L. Miller, S. Moeller, S. Petersen, J. Power, G. Salimi-Khorshidi, A. Z. Snyder, A. T. Vu, M. W. Woolrich, J. Xu, E. Yacoub, K. Uğurbil, D. C. Van Essen, and M. F. Glasser, "Resting-state fmri in the human connectome project," *NeuroImage*, vol. 80, pp. 144–168, 2013. Mapping the Connectome.

[22] R. C. Craddock, G. James, P. E. Holtzheimer III, X. P. Hu, and H. S. Mayberg, "A whole brain fmri atlas generated via spatially constrained spectral clustering," *Human Brain Mapping*, vol. 33, no. 8, pp. 1914–1928, 2012.